Robust Design of a Re-entry Unmanned Space Vehicle by Multi-fidelity Evolution Control

Edmondo Minisci
School of Engineering, University of Glasgow
James Watt South Building, G12 8QQ
Glasgow, UK
edmondo.minisci@glasgow.ac.uk

Massimiliano Vasile
Department of Mechanical Engineering,
University of Strathclyde
75 Montrose Street, G1 1XJ
Glasgow, UK
massimiliano.vasile@strath.ac.uk

ABSTRACT

This paper addresses the preliminary robust design of a small-medium scale re-entry unmanned space vehicle. A hybrid optimisation technique is proposed that couples an evolutionary multi-objective algorithm with a direct transcription method for optimal control problems. Uncertainties on the aerodynamic forces and vehicle mass are integrated in the design process and the hybrid algorithm searches for geometries that minimise the mean value of the maximum heat flux, the mean value of the maximum achievable distance, and the variance of the maximum heat flux. The evolutionary part handles the system design parameters of the vehicle and the uncertain functions, while the direct transcription method generates optimal control profiles for the re-entry trajectory of each individual of the population. During the optimisation process, artificial neural networks are used to approximate the aerodynamic forces required by the direct transcription method. The artificial neural networks are trained and updated by means of a multi-fidelity, evolution control approach.

Track: Evolutionary Multiobjective Optimization

Categories and Subject Descriptors

J.2 [**Physical Sciences and Engineering**]: Aerospace, Engineering; G.1.6 [**Numerical Analysis**]: Optimization

General Terms

Algorithms, Design

Keywords

Multi-Objective Evolutionary Algorithms, Robust Multi Disciplinary Design, Meta-modelling, Optimal Control, Unmanned Space Vehicles

GECCO'11, July 12–16, 2011, Dublin, Ireland.

1. INTRODUCTION

The increase in computer performance allows numerical simulation to replace a big portion of experimental tests, and numerical optimisation to handle complex multidisciplinary design problems. However, generally only reduced or low-fidelity models are used during the optimisation process on sequential machines. Higher fidelity models are used only for more detailed investigations of some promising configurations. In order to reduce the duration and cost of the design process, it would be desirable to introduce high fidelity models already in the preliminary design phase. New methodologies and techniques are therefore required to efficiently handle time consuming, high fidelity models.

In order to be useful and complete, an approach should be able to 1) integrate system design and optimal control, and 2) efficiently incorporate design uncertainties in the optimisation process.

This paper presents a novel approach, to the preliminary robust design of complex engineering systems, that integrates system design and optimal control into a single optimisation process. A population of individuals evolves multiple system design solutions in parallel using an Estimation of Distribution Algorithms (EDAs)[17] called MOPED (Multi-Objective Parzen based Estimation of Distribution) algorithm[8, 3]. At every step of the evolution, an optimal control profile is associated to each individual of the population (each system design solution). The optimal control profile is generated by solving an optimal control problem with a direct transcription method (for more details on transcription methods for optimal control the interested reader can refer to [4]). Uncertainties in the system design parameters are propagated through the model to compute mean and variance of the relevant performance indexes. Mean and variance are then used as objectives for MOPED. Finally, a meta-modelling technique is used to reduce the computational costs of expensive models.

The case study considered in this paper is the robust design of a medium scale Unmanned Space Vehicle (USV). USVs are seen as a test-bed for enabling technologies and as a carrier to deliver and return experiments to and from low-Earth orbit. They are a potentially interesting solution also for the exploration of other planets or as long-range reconnaissance vehicles [22, 24, 21].

In [19] the authors describe a similar approach applied to the design of a small scale USV, taking into account the availability of last generation thermal protection systems (TPS) based on ultra-high temperature ceramic materials

(UHTC)[30, 27]. Here the integrated technique is applied to the design of a medium scale USV, considering a more complex implementation, with two different trajectory optimisations: different control laws allow the same vehicle to follow a) the path that minimises the maximum heat flux, and b) the one maximising the orthodromic distance, during the re-entry phase. As in [19], here the shape of the vehicle is derived from on an ideal waverider configuration ([29, 15, 28]), and its geometry is modified in order to introduce more realistic rounded edges.

An Artificial Neural Network (ANN) approximator is used to reduce the cost of aerodynamic computations. During the optimisation process, the aerodynamic database used to generate the meta-model is updated by a multi-fidelity approach [20, 26, 10, 7, 6]. In particular, low-fidelity models are used to generate samples globally over the range of the design parameters, while high fidelity ones will be used to locally refine the meta-model in later stages of the optimisation.

The paper starts by describing the aerodynamic, thermal, mass, and dynamic models of the vehicle, and detailing the robust multidisciplinary design approach, together with the meta-modelling integration, and treatment of model uncertainties, which are the most innovative aspects of the whole approach. Then the algorithm setting and implementation for the USV test case, and some preliminary results are described and discussed.

2. USV SYSTEM MODELS

This section introduces all system models used to compute the characteristics of the vehicle: geometry, aerodynamic forces, heat flux, mass, dynamics and kinematics.

2.1 Geometry and Shape Model

The vehicle is a modified version of a waverider with rounded edges. The waverider baseline geometry is defined by three two-dimensional power-law equations[28]. The planform and the upper surfaces of the vehicle are parameterised by the length l, the width, w, a power law exponent n, the vehicle centre line wedge angle, θ, and β, which is the oblique shock wave inclination angle[28]. More details can be found in the cited reference.

2.2 Aerodynamic Models

Two different models are used to predict the aerodynamic characteristics of the vehicle. The former one is a simplified analytical model, which is here applied to the actual rounded-edge vehicle, although it was originally developed to predict the aerodynamics of the original sharp-edge shape of the waverider configuration[28]. It gives a very first approximation of the performance at the early stage of the design process. The latter one is a full high-fidelity computational fluid dynamic (CFD) model based on a finite volume integration of Reynolds Averaged Navier-Stokes equations (RANS).

The analytic model gives the lift L and wave drag D_w as functions of the pressure on the upper, lower and base surfaces, with the pressure on the surfaces calculated analytically with the oblique shock theory or Prandtl-Meyer expansion theory[5]. While the viscous drag D_v is given in analytical form, by using the reference temperature method[31]. This simplified model, developed for sharped shape of the waverider, has been modified here to take into account the rounded edges, by considering into the expressions the effective dimension of the lower, upper, and base surfaces.

On the other hand, a commercial code ($Numeca^{®}$), solving the Reynolds Averaged Navier-Stokes (RANS) equations, is used to obtain what are considered high fidelity solutions in the entire flight envelope and also to compute initial solutions when the analytical model could not be applied (for supersonic flight regimes).

The computational domain is discretised by a multi-block structured mesh made by 13 blocks with near 2.4 10^6 total nodes. For each configuration, the mesh is changed and adapted to the current geometry by internal scripting on the basis of design parameters. Since no out of plane flight conditions are considered, only half of the actual domain is discretised and mirror plane conditions are imposed into the longitudinal plane.

Two different settings are implemented and used during the process:

- Laminar for Reynolds number, Re, $< 0.95\ 10^5$
- Fully turbulent (no transition model is considered) for $Re > 1.05\ 10^5$

For hypersonic conditions the radiative equilibrium temperature at the nose is imposed on the solid boundaries. Real gases database is enhanced on the basis of reported air data for high temperatures [2].
No solutions are computed for $0.95\ 10^5 \leq Re \leq 1.05\ 10^5$, in order to have an aerodynamic database as smooth as possible: since there is no transition model between laminar and turbulent flow, then computations into the transition region could be misleading. The data base will be approximated by a smooth ANN system, then the ANN itself will provide smooth approximations for the transition region.

2.3 TPS and Thermal Model

The thermal protection system (TPS) is assumed to be made of Zirconium Diboride (ZrB_2) UHTC, which has following properties: density = $6000 kg/m^3$, specific heat = $628 JKg^{-1}K^{-1}$, conductivity = $66 Wm^{-1}K^{-1}$, and emissivity = 0.8.

We bound the angle of attack to a maximum value of 20 deg, hence the highest heat flux is expected to be at the USV nose cap. Thus, the whole nose cone is made of UHTC with length L_{TPS}. The rest of the vehicle is covered with a thin shell with a constant thickness of 0.003 m.[23]

For the design process, the convective heat flux is computed in the simplest way, with the analytical formula[1]:

$$\dot{q}_{conv} = K_e \sqrt{\frac{\rho_\infty}{R_n}} V_\infty^3 \tag{1}$$

where $K_e = 1.742\ 10^{-4}$ (for the heat flux $\dot{q}_{conv}$ in W/m^2).

2.4 Mass Model

The total mass of the vehicle is made of the structural mass m_{st}, the mass of the TPS m_{TPS}, and the mass of the payload (avionics and power system) m_{pl}.

$$m = m_{TPS} + m_{st} + m_{pl} \tag{2}$$

The mass of the payload is here assumed to be 40% of the structural mass, therefore $m_{pl} = 0.4\, m_{st}$. The mass of the TPS is made of the mass of the nose $m_{nose} = \rho_{TPS} V_n$ plus

the mass of the thin skin covering the rest of the vehicle m_{skin}, where V_n, is the volume of the nose and ρ_{TPS} the density of the TPS material. The mass of the TPS skin covering the vehicle, except the nose, is:

$$m_{skin} = \rho_{TPS}\, S_{TPS}\, d_{TPS} \tag{3}$$

where d_{TPS} is the thickness of the TPS , and S_{TPS} is surface area except that of the nose, which can be approximated by $S_{TPS} = 2S_{pE}+S_{bE}-S_n$ (S_{pE} and S_{bE} are the total planform surface and the area of the rear part of the rounded edge waverider, respectively, and S_n is the surface of the TPS nose).

The structure of the vehicle is supposed to be made of titanium, with a density of 4400 kg/m^3. The structural mass m_{st}, can be obtained from:

$$m_{st} = \rho_{body}(2S_{pE} + S_{bE})d_{boby} \tag{4}$$

where, in this case, d_{boby}= 0.005 m is the thickness of the structure of the vehicle, seen as a shell.

2.5 Dynamic Equations

The vehicle is considered to be a point mass, whose motion is governed by the following set of dynamic equations[14]:

$$\begin{cases} \dot{r} = vsin\theta_p \\ \dot{\lambda} = \dfrac{vcos\theta_p cos\xi}{rcos\phi} \\ \dot{\phi} = \dfrac{vcos\theta_p sin\xi}{r} \\ \dot{v} = -\dfrac{D(\alpha)}{m} - gsin\theta_p \\ \dot{\theta}_p = \dfrac{L(\alpha)}{mv}cos\gamma_v - (\dfrac{g}{v} - \dfrac{v}{r})cos\theta_p \\ \dot{\xi} = \dfrac{L(\alpha)}{mvcos\theta}sin\gamma_v - \dfrac{v}{r}\cos\theta_p\cos\xi\tan\phi \end{cases} \tag{5}$$

where r is the norm of the position vector with respect to the centre of the planet, λ is the longitude, ϕ the latitude, v the magnitude of the velocity, θ_p is the flight path angle, ξ is the heading angle (azimuth of the velocity). No out of plane manoeuvres are considered, thus γ_v is kept equal to zero during the whole trajectory.

3. ROBUST MULTIDISCIPLINARY DESIGN APPROACH

The objective of the design process is to find the shapes of a USV allowing to minimise the maximum heat flux and maximise the distance during a re-entry mission. This design process requires the simultaneous optimisation of the shape and trajectory control profiles of the vehicle, since both of them have an impact on the performance.

The considered approach hybridises an evolutionary multi-objective algorithm with a direct transcription method for optimal control problems, where the external multi-objective evolutionary code manages the parameters defining the shape and considers as objective and constraint functions the statistical characteristics of the responses of two internal optimisation processes. The optimal control problem is solved twice: first the optimal control law is found considering the maximum heat flux as performance index, and mean values and variances of maximum heat flux and orthodromic distance are computed following the procedure described in section (3.1), then an analogous problem is solved considering the negative value of the orthodromic distance as performance index (the solver minimises) and, again, the mean values and variances of maximum heat flux and orthodromic distance are computed

The trajectory optimisation part of the algorithm relies on an artificial neural network system, which approximates the aerodynamic forces acting on the vehicle as functions of the shape of the vehicle and its operative conditions. In order to reduce the computational costs related to the training and updating of the ANNs, a multi-fidelity evolution control approach is adopted.

Following sections detail the different aspects of the approach.

3.1 Robust Design Optimisation Under Uncertainty

Optimal control subproblems consider deterministic models and, consequently, give deterministic values of the performance indexes, $\max_t \dot{q}$ and $Dist$, as a function of the optimal α profiles. However, a number of elements can be considered uncertain, such as the aerodynamic forces and the mass.

Therefore, one can associate to the nominal value of lift L_{det} and drag D_{det}, the uncertain quantities:

$$\begin{aligned} L_{unc} &= L_{det} + Err(\alpha, v, H)C_E(\alpha, v, H)L_{det} \\ D_{unc} &= D_{det} + Err(\alpha, v, H)C_E(\alpha, v, H)D_{det} \end{aligned} \tag{6}$$

where Err is an error function, which depends on the angle of attack, the speed and the altitude H, and C_E is a parametrised sampling hyper-surface which maps a triplet of values of angles of attack, speed and altitude into the interval $[-1, 1]$. Since the idea is that the uncertainties of the aerodynamic data increase with the angle of attack, speed, and altitude, then Err is modelled here as a linear 3D surface, with values that vary from 0.2, when angle of attack, speed and altitude are = 0, to 0.8, when the incidence is = 20 deg, the speed is = 8000 m/s and the altitude is 100 km. The total mass is considered uncertain as well, and it is supposed that m can uniformly vary in the range ± 0.1 of the reference value.

Thus, given a nominal trajectory with an optimal control profile α^*, N_s trajectories are re-propagated. For each one of the N_s trajectories a different C_E surface is built on the basis of sampled random parameters and a new value of the mass is sampled in the neighbourhood of the deterministic value, as well. Then, the mean values and the variances of the performance indexes are computed on the basis of the results of the randomised re-propagation and eventually used as performance indexes for the external loop, which optimises the shape. If we call $E_{q,1}$ and $\sigma^2_{q,1}$ the mean value and variance of maximum heat flux, and $E_{D,1}$ and $\sigma^2_{D,1}$ the mean value and variance of the orthodromic distance after the first control optimisation, and $E_{q,2}$, $E_{D,2}$, $\sigma^2_{q,2}$, $\sigma^2_{D,2}$ the corresponding values after the second control optimisation, then the external process is set as:

$$\min_{\mathbf{d}\in D}[E_{q,1},\ E_{D,2},\ \sigma^2_{q,1} + \sigma^2_{q,2}] \tag{7}$$

subject to the following constraints:

$$\begin{cases} E_{q,1} \le \bar{E_q} \\ (\sigma^2_{q,1} + \sigma^2_{q,2}) \le \bar{\sigma^2_q} \end{cases} \tag{8}$$

while the design vector $\mathbf{d}$ is defined as $\mathbf{d} = [l, w, n, \theta, R_n, \Delta\dot{q}]$ (the meaning of $\Delta\dot{q}$ is explained in the next section).

3.2 Multi-objective Algorithm

The external Multi-objective optimisation (MOO) problem (7)is solved with a particular type of evolutionary algorithm which belongs to the sub-class of Estimation of Distribution Algorithms (EDAs)[17].

The specific EDA employed in this work is derived from the MOPED (Multi-Objective Parzen based Estimation of Distribution) algorithm[8, 3]. MOPED is a multi-objective optimisation algorithm for continuous problems that uses the Parzen method to build a probabilistic representation of Pareto optimal solutions, with multivariate dependencies among variables. Non-dominated sorting and crowding operators[9] are used to classify promising solutions in the objective space, while new individuals are obtained by sampling from the Parzen model.

The Parzen method[12] is a non-parametric approach to kernel density estimation, which gives rise to an estimator that converges everywhere to the true Probability Density Function (PDF) in the mean square sense. Should the true PDF be uniformly continuous, the Parzen estimator can also be made uniformly consistent. In short, the method allocates exactly n_k identical kernels, each one centred on a different element of the sample. More details on the original code can be found in the cited works. In the next section, the trajectory optimisation code and the evolution control technique with multi-fidelity approach are detailed.

3.2.1 Trajectory Optimisation

For the trajectory optimisation problem, the control variable is the angle of attack α, therefore the control laws are the result of two optimal control subproblems as:

$$\min_{\alpha} \max_{t} \dot{q} \quad and \quad \max_{\alpha} Dist \tag{9}$$

both subject to dynamic equations (5) and terminal conditions:

$$\begin{cases} r(t=0) = r_0 \\ \lambda(t=0) = \lambda_0 \\ \phi(t=0) = \phi_0 \\ v(t=0) = v_0 \\ \theta_p(t=0) = \theta_0 \\ \xi(t=0) = \xi_0 \end{cases} \tag{10}$$

$$\begin{cases} r(t=t_f) \leq r_f \\ r(t=t_f) \geq r_{min} \\ v(t=t_f) \leq v_f \\ v(t=t_f) \geq v_{min} \end{cases} \tag{11}$$

These problems are transcribed with a Gauss pseudospectral method[11]: the trajectory is decomposed in N elements, each of which has n_p collocation points. After transcription, the optimal control problems defined by (9), (5) and (10, 11) become the following general nonlinear programming problem:

$$\min_{\alpha_s} \max_{t} \dot{q} \quad and \quad \max_{\alpha_s} Dist \tag{12}$$

subject to the nonlinear algebraic constraints:

$$C(r_s, \lambda_s, v_s, \xi_s, \theta_s, \alpha_s, t_s) = 0 \tag{13}$$

and the terminal constraints (10, 11).

where $r_s,\ \lambda_s,\ \phi_s,\ v_s,\ \xi_s,\ \theta_s,\ \alpha_s,\ t_s$ are the discrete values of the time, states and control values at the nodes of the transcription scheme. In order to obtain feasible and re-integrable solutions, an inequality constraint on the variation of the control law is also imposed: for each node the slope of the control law $\leq \Delta\alpha$.

Note that the second optimisation problem takes into account an additional constraint on the maximum heat flux, which should be $\leq (\dot{q}_{max,1} + \Delta\dot{q})$, where $\dot{q}_{max,1}$ is the deterministic value of the maximum heat flux resulting from the previous control law optimisation, and $\Delta\dot{q}$ is a variable of the problem, managed by the external evolutionary process.

The re-entry time is free and no other terminal conditions are imposed as there is no specific requirement on the landing point.

The NLP problem was solved with the Matlab® function *fmincon*, with *interior-point* solution algorithm.

3.3 Multi-fidelity Evolution Control

The basic idea underneath evolution control (EC) approaches is to use, throughout the optimisation process, both the true and the surrogated models in a way that reduces the total computational time, without loosing in precision.

Due to the necessity to limit the number of training samples, it is very difficult to construct an initial approximated model that is globally correct. Most likely, the approximation will bring the optimisation algorithm to false optima, i.e. solutions that are optimal for the approximated model but are suboptimal for the true functions.

Model management or evolution control techniques address this problem and avoid finding false optima, or missing true ones.

Jin et al[16] in their paper propose two different approaches for the evolution control of the model: a) individual-based control and b) generation-based control. In the first approach, n_v individuals in the current population are chosen and evaluated with the true model at each generation. In the latter, the whole population is evaluated with the real model, every n_{gcyc} generations, for n_{gv} generations, where $n_{gv} < n_{gcyc}$. The individuals evaluated with the true model are then introduced into the dataset in order to locally improve the surrogated model in the promising regions.

The method here is a mix of both evolution control strategies. Fig. 1 summarises the whole optimisation process. The MOO optimisation algorithm MOPED is integrated with an external procedure that monitors the status of the approximated models. At the end of each iteration (generation), the external procedure checks if an updated version of the approximated model is ready and available. If the approximated model is updated, then all the individuals in the current population are re-evaluated and re-classified with the updated model, before the Parzen distribution is updated and sampled. If the approximated model is not updated, because, for example, a CFD computation is still running, and the difference between the generation of the previous update and the current generation is n_{gcyc}, then MOPED pauses and waits for the new update.

In an asynchronous way, an additional external procedure (bottom right block in Fig. 1) manages the training and up-

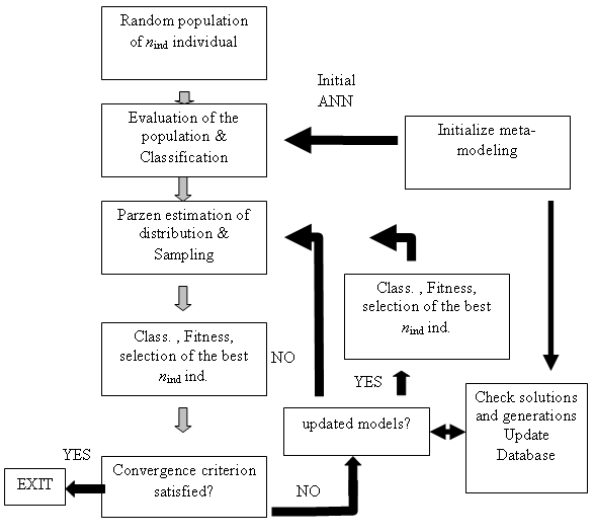

Figure 1: MOPED with evolution control modification and independent approximator handler.

dating of the approximated model. This procedure needs as input a list of system models ordered by increasing level of fidelity and a scheduling report detailing how and when the different models should be used. Then it extracts for each optimal trajectory the matrix $\mathbf{S}_{opt} = [l, w, n, \theta, R_n, \mathbf{v}, \mathbf{H}, \alpha]$. Each row in matrix $\mathbf{S}$, composed by the 5 geometrical parameters and the operative point along the trajectory, is then compared to the values in $\mathbf{DB}_{train}$, which is the matrix of points in the database used to train the ANNs. The procedure works as follows:

- At generation 0, it trains a first ANN system using the low-fidelity model (fidelity level 0) and then passes the ANNs to MOPED (process *Initialise App 0* in figure 1); $\mathbf{DB}_{train}$ is initialised;
- At each subsequent generation:
  1. Initialise counter $i_c = 0$;
  2. while $i_c <= n_t$
     (a) extract from the population a sampled trajectory and extract n_o operative points;
     (b) for i = 1 ... n_o
     - compute the minimum Euclidean distance $d_{sl,i} = min_j \|S_{opt,i} - DB_{train,j}\|$ where j loops over all the points in the database (the rows of DB_{train});
     - if $d_{sl,i} > d_{min,sl}$ then the point $S_{opt,i}$ is evaluated and immediately inserted into the database DB_{train}, and $i_c = i_c + 1$; all the solutions in the database that were computed with a lower fidelity model and have $d_{sl} < d_{min,ll}$ are discarded from future updates of the approximating model;
     - if $i_c = n_t$ interrupt loops
- Every n_{gl} generations of the global optimizer, it increases the level of fidelity of the model, till the maximum level is reached.

It can be argued that the data obtained by the higher fidelity models progressively become the main source of updates for the neural networks till, near the end of the optimisation process, the influence of the data obtained by the lower fidelity models is practically nullified in the optimal region.

3.4 Surrogate Model

General principles of evolution control do not depend on any specific approximation technique but, of course, the approximation approach strongly affects the outcome of any EC strategy. Due to the particular task, the approximator should be able to filter the noise of the CFD models responses and should be able to correctly generalise in the broad range of shape parameters and operative conditions. Response surfaces and artificial neural networks were considered[25, 13], but ANNs have been preferred, because they are more robust and generally useful when there is no information on the general structure of the function to approximate.

When dealing with ANNs, usually radial basis NNs are preferred due to the modest computational effort required to train them [25, 13], but here the generic Multi Layer Perceptron (MLP) ANN with one hidden layer was used, due to the expected better generalisation in regions *far* for the training data.

The training process is based on a Bayesian regularisation back-propagation[18], which limits any overfitting problem, and the idea is that the computational costs of initial training and online update are negligible if compared to the calls to the high-fidelity model.

In this case, the 8 inputs to the ANN approximators (two distinct ANNs are used to approximate the lift and the drag) are: the 5 geometric parameters (l, w, n, θ, and R_n), the angle of attack, α, the speed, v, and the altitude H (defined $H = r - R_E$, where R_E is the mean radius of the Earth). The outputs are the coefficients of lift, C_L and drag, C_D. The networks are trained to reach a mean squared error of 1% on the normalised training output.

It should be noted, that in this case the approximator does not directly approximate the objective and/or constraint functions, but it is used to obtain a cheap aerodynamic surrogate model of the system, which is necessary to solve the optimal control subproblems.

4. OPTIMISATION SET AND RESULTS

The design space for problem (7) is defined by the following bounds on the design parameters: the nominal length $l \in [2.9, 4.2][m]$, the nominal width $w \in [1.0, 2.0][m]$, the exponent $n \in [0.2, 0.7]$, the angle $\theta \in [7, 11][deg]$, the radius of the nose $R_n \in [0.01, 0.04][m]$, the constraint on the maximum heat flux for the second control law optimisation $\Delta\dot{q} \in [20, 70][W/cm^2]$. The angle β, as defined in section 2.1, is kept fixed to $12deg$. Moreover, here L_{TPS} is not considered as a design parameter, and its value is set as 10% of the effective length of the vehicle.

The constraints on the external process are: $\bar{E}_q = 180$ and $\bar{\sigma^2_q} = 1000$.

The trajectories are discretised with 6 elements, and 12 nodes are considered for the first 3 elements (from starting point to half of the trajectory path), where maximum values of the heat flux and major trajectory oscillations are expected, while 5 nodes are considered the other 3 elements.

The bounds on the variables of the trajectory optimisation are: total time $T_{tot} \in [500, 6500]$ $[s]$, angle of attack $\alpha \in [0, 20]$ $[deg]$, radius $r \in [6.380\ 10^6, 6.480\ 10^6][m]$, longitude $\lambda \in [-180, 21]$ $[deg]$, latitude $\phi \in [-90, 68]$ $[deg]$, speed $v \in [100,\ 10^4]$ $[m/s]$, flight path angle $\theta_p \in [-80, 10]$ $[deg]$, heading angle $\xi \in [-225, -90]$ $[deg]$.

The initial conditions (10) are $x_0 = [R_E + \ 10^5,\ 21,\ 68,\ 7700,\ -0.3,\ -145]^T$, where R_E is the mean radius of the Earth, while the constraints on the final conditions are $r_f = R_E + 50000$ m, $r_{min} = R_E + 15000$ m, $v_f = 1100$ m/s, $v_{min} = 900$ m/s, while the slope of the control law is $\Delta\alpha = 1/10$ deg/s. The initial guess of the control law for every individual had 18 deg incidence at time $t = 0$, linearly decreasing, with decrements $d\alpha = 1/1000$ deg/s, till the last point of the trajectory obtained by direct integration satisfies the constraints on the required final velocity and altitude.

The MOO process was run for 60 generations with a population of 60 individuals. The initial approximators were built with 1000 samples, selected with a randomised Latin Hypercube, coming from 920 analytic model computations and additional 80 supersonic CFD computations to have an extended range of validity, without the need to excessively extrapolate. The computation of the first database required nearly 1200 hours of computational time, distributed on a cluster of 20 linux64 processors (near 3 days of effective time). The computations of the CFD solver were stopped when convergence was obtained on the aerodynamic forces.

The characteristic parameters of the evolution control process were set as follows: $n_t = n_o = 20$, $n_{gl} = 10$, with only 1 switch; $n_{gcyc} = 5$; $d_{min,sl} = 0.3$ (all the inputs are normalised to $[-1, 1]$); $d_{min,ll} = 0.8$.

At level 0, which is considered up to generation 10, CFD computations were used to verify only supersonic points, while at level 1, which is considered from generation 11, CFD computations were used to verify the trajectory points for the whole trajectory.

During the computation, until generation 50, the solutions obtained with the CFD model increased up to 250, allocated in the promising region of the search space, while the analytical ones, used to build the ANN approximators, decreased to nearly 500. From generation 50 to 60 no more new verified values are added to the ANN database.

The approximation of the Pareto front at the end of the optimisation process is shown in Fig. 2. As expected, the front is sparse and irregular, due to the nature of the objective functions, which are extremely noisy because they are the outcome of the Monte-Carlo sampling ($N_s = 300$, then each individual required 600 re-propagations), which also rely on the control law obtained from the internal optimisation process. Moreover, the speed and accuracy of convergence of the trajectory optimisation loop is quite sensitive to shape parameters and initial conditions. A different population size could improve the quality of the front although a trade-off between exhaustiveness of the search and computational resources is required.

In Fig. 3 individuals A, B, and C minimise the mean value of the maximum heat flux, maximise the mean value of the distance, and minimise the sum of the variances, respectively.

The design parameters for solutions A, B and C are:

- Solution A: $l = 2.93998; w = 1.19734; n = 0.6977; \theta = 9.9983; R_n = 0.03532; \Delta\dot{q} = 41.9184$

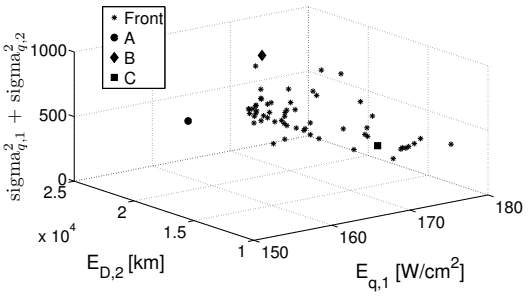

Figure 2: Approximation of the Pareto Front at the end of the optimisation process

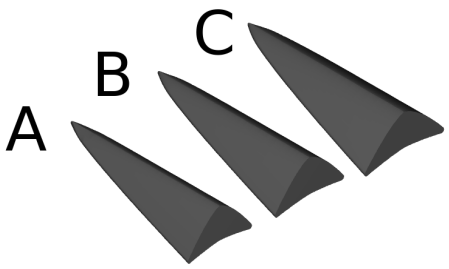

Figure 3: Optimal solutions: individual A minimises the mean value of the maximum heat flux, individual B maximises the mean value of the achievable distance, while individual C minimises the sum of the variances.

- Solution B: $l = 2.98669; w = 1.28207; n = 0.6871; \theta = 10.4961; R_n = 0.03719; \Delta\dot{q} = 62.6298$

- Solution C: $l = 3.12287; w = 1.49396; n = 0.6999; \theta = 9.7599; R_n = 0.03913; \Delta\dot{q} = 33.8409$

The optimisation is mainly driven by the easiest way to fulfil the requirements. In order to limit the heat flux at the nose, the code follows a path bringing to solutions with a relatively big radius of the nose, and at the same time to solutions with small dimensions. Since the total mass is strictly related to the size, the code answers with small and light vehicles, which are able to surf avoiding the very critical part of the flight envelope.

Figure 4 shows the nominal, deterministic trajectories of the three selected individuals, when the control law is optimised taking into account the maximum heat flux as performance index. The shapes of the individuals are very similar, but the smaller size, meaning a smaller mass as well, allows individual A to follow a higher re-entry path in the critical part of the trajectory, limiting the heat loads (figure 5) (the masses of individuals A, B, and C are 191, 212, 248 kg, respectively).

Performance of the individuals are also strongly influenced by the convergence of the control law optimisation, which can get stuck into local minima and give substantially different results for similar shapes, as can be seen in figure 6, where the angle of attack is plotted against time.

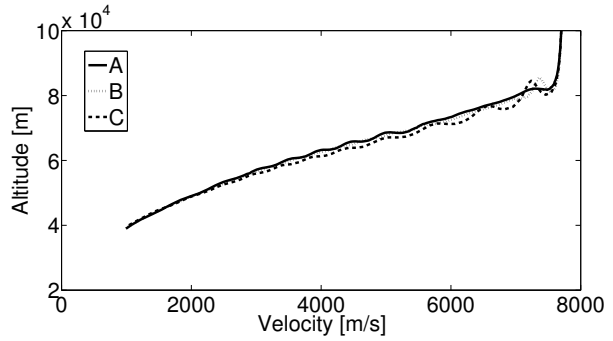

Figure 4: Trajectories of the selected optimal solutions.

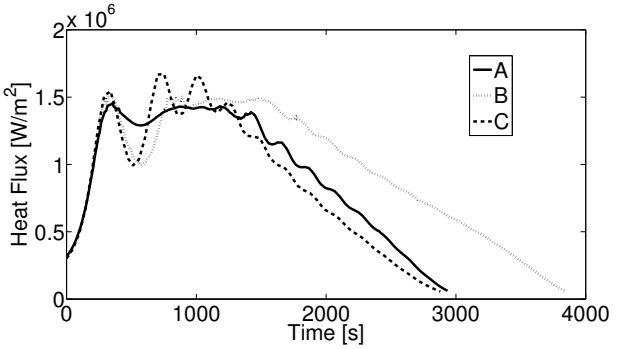

Figure 5: Convective heat flux of the selected optimal solutions.

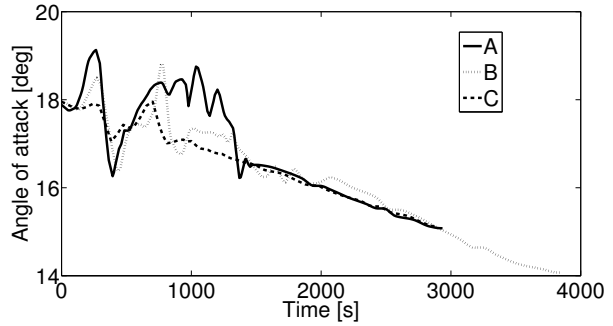

Figure 6: Angle of attack control law.

In order to understand the design margins obtained by the robust optimisation process, a second bi-objective optimisation, which directly considers the nominal/deterministic values of the maximum heat flux and the orthodromic distance as objectives, has been carried out (same settings of the robust one). The obtained approximation of the front is shown in figure 7, and compared to a 2D projection of the robust front. As expected the process is able to find solutions with smaller (better) values of the maximum heat flux (left part of the figure), which, in the robust case, are not Pareto optimal because of the third objective function. It has to be noted, however, that this particular run is not capturing the part of the front, which should be expected above individuals A and B. This lack of coverage is due to the stochastic nature of the process and the noise in the model. A full comparison between deterministic and robust solution would require multiple runs, which is currently prohibitive.

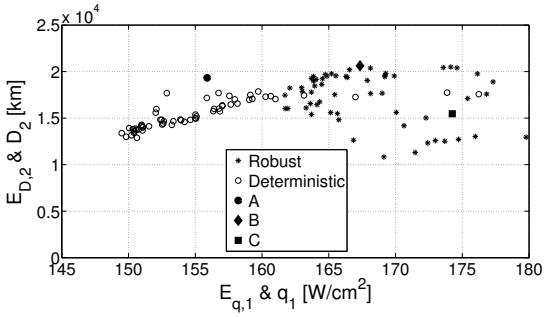

Figure 7: Comparison between robust and deterministic optimisation processes.

5. CONCLUSIONS

This paper describes a novel evolutionary approach to integrate system design and optimal control into a single optimisation process. The procedure implements a combination of a global, population based solver with a direct transcription method for optimal control problems.

The test case considered here is the robust design of a small scale USV for re-entry operations. The control problem solver is interfaced with an ANN system, approximating the aerodynamic forces as a function of the geometric parameters and operational conditions, which is trained and upgraded by a form of evolution control. The evolution control procedure considers a multi-fidelity approach that incorporates uncertainties on the response of some of the models.

The model presented in this paper is not fully comprehensive of all the aspects defining the system and phenomena occurring during the re-entry phase, nonetheless it has the main characteristics of a real, complex case, such as: the system and optimal control components are integrated in a multilevel design optimisation process, both system and optimal control design processes are computationally expensive and very noisy.

In the future the approach will be tested on more realistic re-entry problems and generalised to solve analogous problems in other engineering fields, e.g. the design of chemical plants and the design of high performance cars for predefined circuits, also with higher number of shape design variables, at the limits of the meta-modeling capabilities.

Current work mainly focuses on the improvement of the aero-thermodynamic model and finding a way to insert into the process also very expensive unsteady computations, likely only for few points of the flight envelope and/or to better assess the errors and consequent uncertainties when lower fidelity level models are adopted. The uncertainty modelling is currently one of the most critical aspects of the system and needs to be improved including knowledge coming from the expected error of the approximator and convergency level of the CFD results.

Another important aspect to consider for future improvements is the convergence of the internal optimal control solver, which strongly affects the results.

6. REFERENCES

[1] J. Anderson. *Hypersonic and High-Temperature Gas Dynamics (Second Edition)*. AIAA, 2006.

[2] B. Aupoix and J. Cousteix. Real gas effects in two- and three-dimensional hypersonic, laminar boundary layers. In T. Murthy, editor, *Computational Methods in Hypersonic Aerodynamics*, pages 293–340. Kluwer Academic Publishers, 1991.

[3] G. Avanzini, D. Biamonti, and E. Minisci. Minimum-fuel/minimum-time maneuvers of formation flying satellites. In *Astrodynamics Specialist Conference*, AAS 03-654, Big Sky, Montana, 03-07 August 2003.

[4] J. T. Betts. *Practical Methods for Optimal Control and Estimation Using Nonlinear Programming, Second Edition*. SIAM, 2010.

[5] C. Chapman. *High speed flow*. Cambridge University Press, 2000.

[6] S. Choi, J. Alonso, and I. Kroo. Two-level multifidelity design optimization studies for supersonic jets. *Journal of Aircraft*, 46(3):776–790, 2009.

[7] S. Choi, J. Alonso, I. Kroo, and M. Wintzer. Multifidelity design optimization of low-boom supersonic jets. *Journal of Aircraft*, 45(1):106–118, 2008.

[8] M. Costa and E. Minisci. MOPED: a Multi-Objective Parzen-based Estimation of Distribution algorithm. In C. Fonseca, P. Fleming, E. Zitzler, K. Deb, and L. Thiele, editors, *Evolutionary Multi-Criterion Optimization. Second International Conference, EMO 2003*, volume 2632 of *LNCS*, pages 282–294, Faro, Portugal, 08-11 April 2003. Springer.

[9] K. Deb, A. Pratap, S. Agarwal, and T. Meyarivan. A Fast and Elitist Multiobjective Genetic Algorithm: NSGA-II. *IEEE Transaction on Evolutionary Computation*, 6(2):182–197, april 2002.

[10] J. J. Doherty, S. R. H. Dean, P. Ellsmore, and A. Eldridge. A multi-fidelity approach for supporting early aircraft design decisions. In R. Curran, S. Y. Chou, and A. Trappey, editors, *Collaborative Product and Service Life Cycle Management for a Sustainable World*, pages 267–279. Springer London, London, 2008.

[11] B. Fornberg. *A Practical Guide to Pseudospectral Methods*. Cambridge University Press, 1998.

[12] K. Fukunaga. *Introduction to statistical pattern recognition*. Academic Press, 1972.

[13] K. Giannakoglou. Design of optimal aerodynamic shapes using stochastic optimization methods and computational intelligence. *Progress in Aerospace Sciences*, 38:43–76, 2002.

[14] W. L. Hankey. *Re-entry Aerodynamics (AIAA Education Series)*. AIAA, 1988.

[15] W. Heinze and A. Bardenhagen. Waverider aerodynamics and preliminary design for two-stage-to-orbit missions, part 2. *Journal of Spacecraft and Rockets*, 35(4):459–466, 1998.

[16] Y. Jin, M. Olhofer, and B. Sendhoff. Framework for evolutionary optimization with approximate fitness functions. *IEEE Transactions on Evolutionary Computation*, 6(5):481–494, 2002.

[17] J. A. Lozano, P. Larranaga, and I. Inza. *Towards a New Evolutionary Computation: Advances on Estimation of Distribution Algorithms (Studies in Fuzziness and Soft Computing)*. Springer, February 2006.

[18] D. MacKay. Bayesian interpolation. *Neural Computation*, 4(3):415–447, 1992.

[19] E. Minisci, H. Liqiang, and M. Vasile. Multidisciplinary design of a micro-usv for re-entry operations. In *AIAA Guidance, Navigation, and Control Conference*, AIAA 2010-7968, Toronto, Ontario Canada, 02-05 August 2010.

[20] T. Robinson, M. Eldred, K. Willcox, and R. Haimes. Surrogate-based optimization using multifidelity models with variable parameterization and corrected space mapping. *AIAA Journal*, 46(11):2814–2822, 2008.

[21] G. Russo. Usv program status 2009. In *Proceedings of the 16th AIAA/DLR/DGLR International Space Planes and Hypersonic Systems and Technologies Conference*, Wahington, DC, 2009. AIAA-2009-7269.

[22] G. Russo and P.P. De Matteis. Prora-usv: Two flight mission exploring transonic conditions. In *Proccedings of the 15th AIAA International Space Planes and Hypersonic Systems and Technologies Conference*, Dayton, Ohio, USA, 2008. AIAA 2008-2660.

[23] R. Savino, M. De Stefano Fumo, D. Paterna, and M. Serpico. Aerothermodynamic study of uhtc-based thermal protection systems. *Aerospace Science and Technology*, 9:151–160, 2005.

[24] R. Savino and D. P. M. Serpico. Numerical and experimental investigation of prora usv subsonic and transonic aerodynamics. *Journal of Spacecraft and Rockets*, 43(3):575–584, 2006.

[25] W. Shyy, N. Papila, R. Vaidyanathan, and K. Tucker. Global design optimization for aerodynamics and rocket propulsion components. *Progress in Aerospace Sciences*, 37:59–118, 2001.

[26] G. Singh and R. Grandhi. Mixed-variable optimization strategy employing multifidelity simulation and surrogate models. *AIAA Journal*, 48(1):215–223, 2009.

[27] T. Squire and J. Marschall. Material property requirements for analysis and design of UHTC components in hypersonic applications. *Journal of European Ceramic Society*, 30(1):2239–2251, 2010.

[28] R. P. Starkey and M. J. Lewis. Analytical off-design lift-to-drag-ratio analysis for hypersonic waveriders. *Journal of Spacecraft and Rockets*, 37(5):684–691, 2000.

[29] D. Strohmeyer, T. Eggers, and M. Haupt. Waverider aerodynamics and preliminary design for two-stage-to-orbit missions, part 1. *Journal of Spacecraft and Rockets*, 35(4):450–458, 1998.

[30] A. Viviani and G. Pezzella. Heat transfer analysis for a winged reentry flight test bed. *International Journal of Engineering*, 3(3):330–345, 2009.

[31] F. White. *Viscous Fluid Flow*. McGraw-Hill, New York, 1974.